ACS APPLIED BIO MATERIALS

Open Access

www.acsabm.org

Article

Nanostructured Zirconia Thin Films as a Neurogliomorphic Interface for Neural Cells of Central and Peripheral Nervous Systems

Giorgia Conte,*,† Francesca Borghi,† Chiara Lazzarini, Claudio Piazzoni, Aikaterini Konstantoulaki, Roberta Fabbri, Marco Caprini, Paolo Milani,*,† and Valentina Benfenati*,†

Cite This: *ACS Appl. Bio Mater.* 2026, 9, 8345−8358

Read Online

ACCESS | Metrics & More | Article Recommendations

ABSTRACT: Recent advances in neuroscience have highlighted the central role of glial cells, particularly astrocytes, in regulating neural network activity through calcium-dependent neuron−glia communication. In parallel, nanostructured cluster-assembled materials have emerged as promising candidates for developing brain−machine interfaces because of their biomimetic morphology, mechanotransductive properties, and neuromorphic behavior. Among these, nanostructured zirconium oxide (ns-ZrOx) thin films have recently demonstrated memristive and signal-processing capabilities compatible with biohybrid neural systems, yet their interaction with heterogeneous neuroglial networks remains poorly understood. Here, we investigate the biocompatibility and functional effects of ns-ZrOx interfaces on primary astrocytes and dorsal root ganglion (DRG) neuron−glia co-cultures, comparing nanostructured and flat zirconia substrates. Both substrates supported cellular adhesion, survival, and differentiation. However, ns-ZrOx selectively enhanced glial calcium signaling, increasing transient amplitude and accelerating response kinetics in both central and peripheral glial populations. Our findings identify ns-ZrOx as an active neurogliomorphic interface capable of modulating neuron−glia communication through nanoscale material properties. By bridging glial physiology with neuromorphic nanomaterials, this work supports the development of hybrid bioelectronic platforms integrating living neural networks with adaptive functional materials for brain-inspired computing and advanced neural interfaces.

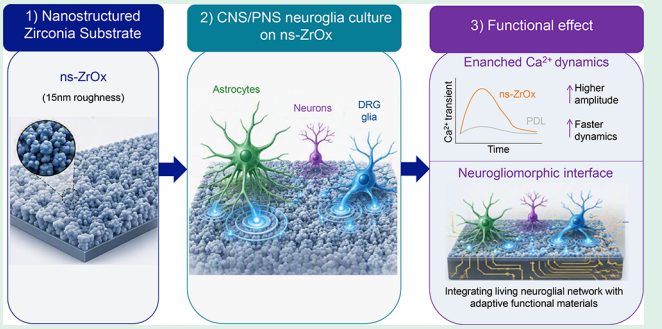

KEYWORDS: *nanostructured zirconia, astrocyte, dorsal root ganglion, calcium signaling, neuron−glia interaction, glia-neuromorphic interface*

■ INTRODUCTION

Recent neuroscientific discoveries have profoundly reshaped our understanding of brain function, underscoring the crucial role of glial cells—particularly astrocytes—in the dynamic regulation of neural circuits.[1,2] Far from being passive support elements, astrocytes actively participate in synaptic transmission, modulate neuronal excitability, and maintain homeostasis through complex bidirectional signaling with neurons.[3,4] Their involvement in synaptic plasticity, metabolic regulation, and even information processing has positioned them as indispensable players in the orchestration of brain network behavior. In particular, intracellular calcium signaling ($[Ca^{2+}]_i$) of astrocytes is central to both neuronal excitability and astrocytic function, acting as a key messenger in synaptic transmission, gliotransmission, and network synchronization.[2,5,6] This paradigm shift highlights an urgent need for a new generation of brain−computer interfaces and devices that rely on materials capable of interacting not only with heterogeneous neuronal elements, such as neurons, but also with glial components. Nanostructured cluster-assembled materials are good candidates to support and interact with heterogeneous neuronal culture, thanks to their mechanotransductive[7−9] and neuromorphic behaviors.[10−12] Mechanotransductive processes are promoted by the nanoscale structure of the cluster-assembled materials and its organization at the mesoscale,[13] with a morphology closely resembling the extracellular matrix (ECM) one,[14,15] thus providing biocompatible and biomimetic surfaces already shown to support neuronal and glial cultures.[7,10] On the other side, the neuromorphic behaviors of nanostructured gold (ns-Au)[13,16] and zirconia (ns-ZrOx) thin films[10,17] allow the development of functional interfaces for the in materia pro-

Received: June 18, 2026
Revised: August 6, 2026
Accepted: August 10, 2026
Published: August 19, 2026

cessing of sensor signals and complex time-series dynamics on rigid[11,18] and soft substrates,[19,20] able to respond to environmental and mechanical stimuli.

The combination of nanostructured zirconia and gold (ns-ZrOx/Au) has recently been shown to exhibit memristive behavior with short-term memory, relaxation dynamics, and spike-dependent plasticity.[10,17] The planar structure of these nanocomposite devices and their biocompatibility make them suitable for the coupling with biological neural networks. Recently, a methodology based on these ns-Au/ZrOx cluster-assembled films and simple statistical analysis methods has proved the feasibility of processing the neural traces recorded by in vivo experiments, without the need for artificial neural networks and preprocessing of the signals.[11] These nanostructured materials are therefore proposed as a potential solution for the implementation of on-edge devices suitable for functional brain–machine interfaces, featuring low energy and computational consumption, and compatible with in vivo applications.[21,22]

In this study, we investigate the biocompatibility and functional properties of neuroglial interfacing of nanostructured zirconia-based films. Specifically, we focused on their application as substrates for co-cultures of glial cells and neurons derived from both the central and peripheral nervous systems. We compare the cellular responses elicited by nanostructured zirconia vs flat zirconia substrates in primary astrocytes and dorsal root ganglion (DRG) neuron–glia co-cultures. Our results reveal robust cellular adhesion, survival, and morphological integration of DRG glia and neurons, as well as the emergence of distinct calcium signaling profiles that vary by cell type and substrate topography.

These findings underscore the capacity of nanostructured zirconia to modulate calcium signaling mediating neuron–glia communication, with implications for its use in next-generation neural interfaces. The observed substrate-dependent differences in calcium dynamics open the path for the use of material surface properties to selectively influence calcium-dependent functional crosstalk between neurons and glia, a hallmark of glia-neuromorphic material interfaces.[2,5,6]

■ MATERIALS AND METHODS

Nanostructured Thin Film Deposition and Characterization

Nanostructured zirconia thin films have been deposited by means of a supersonic cluster beam deposition (SCBD) apparatus,[23] equipped with a pulsed microplasma cluster source (PMCS) for the production of clusters in the gas phase.[24] The SCBD setup schematically consists of two differential pumped vacuum chambers. The first chamber is coupled with a PMCS, where the production of zirconia clusters in the gaseous phase is realized through the ablation of a metal target by a discharge plasma after the injection of an inert gas (Ar). The cluster–inert gas mixture is then extracted to form a supersonic seeded beam that impinges on a glass substrate fixed on a sample holder perpendicular to the beam trajectory in the second chamber. The roughness (Rq) of the nanostructured film evolves with thickness, according to simple scaling laws.[25,26] By recording the film thickness through a quartz microbalance inserted in the deposition chamber, it is possible to finely tune the morphological properties of the film. Flat zirconia samples (Rq ~ 0.2 nm), used as control for the evaluation of the role of morphology, were deposited by ion guns on glass substrates.

Topographical maps of the nanostructured zirconia films have been acquired in air using multimode atomic force microscopy (AFM) equipped with a Nanoscope IV controller (BRUKER). Rigid silicon tapping-mode cantilevers mounting single-crystal silicon tips with a nominal radius 5–10 nm and resonance frequencies in the range of 250–350 kHz have been used. Several 2 μm × 1 μm images were acquired on each sample with scan rate of 1 Hz and 2048 × 512 points. The images were flattened by line-by-line subtraction of first and second order polynomials, in order to remove artifacts due to sample tilt and scanner bow, and subsequently analyzed in Matlab environment.

Rat Cortical Astrocytes Culture Preparation, Maintenance, and Plating

Primary cultures of astrocytes were prepared from newborn Sprague Dawley rat pups (postnatal days P0–P2) following established protocols. Briefly, neonatal cerebral cortices were dissected to remove the meninges, gently triturated, filtered through a 70 μm cell strainer, and plated in T25 flasks. These flasks contained Dulbecco's modified Eagle medium (DMEM) with GlutaMAX, high glucose, 15% fetal bovine serum (FBS), and penicillin–streptomycin at concentrations of 100 U/mL and 100 μg/mL, respectively. The cultures were maintained in a humidified incubator at 37 °C with 5% CO_2. The medium was refreshed every 2 days, and flasks were gently shaken as needed to remove microglial cells. After 2 weeks, when astrocytes reached confluence, cells were detached using 0.25% trypsin–EDTA and re-plated onto flat-ZrOx, ns-ZrOx, and control substrates. Cells were seeded at a density of 5–7 × 10^3 cells per dish and cultured in the medium containing 10% FBS.

Dorsal Root Ganglion Cell Culture Preparation

Primary DRG cultures were prepared from postnatal (P7–P21) rats following established protocols.[27] Equal volumes of the DRG cell suspension were applied directly onto the substrates and incubated at 37 °C in 5% CO_2. DRG cells were maintained in DMEM supplemented with 10% FBS and 50 ng/mL nerve growth factor. Cytosine β-D-arabinofuranoside (AraC, 1.5 mg/mL) was omitted to preserve peripheral glial cell expression.

Cultures were characterized at 3, 5, and 7 days in vitro (DIV) using optical and confocal microscopy.

All experiments adhered to Italian laws governing the protection of laboratory animals and were approved by the Bioethical Committee of the University of Bologna and the Ministry of Health (ID 1268, code number 2DBFE.N.HTT, protocol number 1138/2021-PR). Oversight was provided by the University's veterinary commission to ensure animal welfare. Every effort was made to minimize animal usage and reduce suffering throughout the study.

Fluorescent Diacetate Assay (FDA)

The biocompatibility of astrocytes and DRG neuron–glial cell co-cultures on flat-ZrOx, ns-ZrOx, and PDL (used as a control) was assessed at 3 and 7 days in vitro (DIV) for astrocytes and 5 DIV for DRG using the fluorescein diacetate (FDA) assay. Quantitative analysis was conducted by counting all live, FDA-positive (green) cells/total number of nuclei with ImageJ software.

Differentiation Analysis

Astrocyte differentiation induced by interaction with ZrOx substrates was evaluated using morphological criteria. Cells were classified as differentiated when exhibiting an elongated or star-shaped morphology, while polygonal cells were considered undifferentiated. Quantitatively, a cell was defined as differentiated when the length of its major axis was at least twice that of its minor axis.

Calcium Imaging and Pharmacology

For experiments involving primary cultures, variations in $[Ca^{2+}]_i$ were assessed using calcium microfluorometry with the fluorescent Ca^{2+} indicator Fluo-4 AM (Life Technologies). All calcium imaging experiments were performed on high-density astrocyte cultures (30,000 cells per substrate). Prior to measurements, astrocytes cultured on ZrOx substrates

https://doi.org/10.1021/acsabm.6c01280
ACS Appl. Bio Mater. 2026, 9, 8345−8358

and on PDL were incubated with 2 μM Fluo-4 AM, which was dissolved in a standard bath solution, for 45 min at room temperature.

Measurements of $[Ca^{2+}]_i$ were conducted using a fluorescence microscope (OLYMPUS BX63) equipped with a long-distance water objective (×40) and appropriate filters. Fluorescence was excited using SPECTRA III light engine (Lumencor) at 475/28 nm and collected using a FITC/GFP filter at 525 nm. Camera exposure times were set to 150 ms, with an image sampling rate of 2 Hz. Data acquisition was managed through Metamorph software (Molecular Devices). Blockers were diluted in standard bath saline to achieve their respective final concentrations and were introduced following rinsing. Calcium activity was recorded under basal conditions without application of exogenous agonists or mechanical stimulation. Cells were considered active when spontaneous calcium transients exceeded $\Delta F/F = 0.05$ during the recording period. To analyze the temporal characteristics of $[Ca^{2+}]_i$ dynamics, we calculated the average number of peaks by detecting the fluorescence oscillations recorded over time.

The onset was calculated at the time point where we could measure the minimal variation (0.05 $\Delta F/F$) in $\Delta F/F$.

DRG neurons and glial cells were distinguished based on their morphological characteristics. Neurons and glial cells were identified based on their characteristic morphology during live calcium imaging. Neurons were recognized by their phase-bright, rounded cell bodies and the presence of neuritic processes, whereas glial cells exhibited smaller, flatter cell bodies without long neuritic extensions.

Solution and Chemicals

Salts and other high-purity chemicals were sourced from Sigma. For calcium microfluorometry experiments, the standard bath solution consisted of (mM) 140 NaCl, 4 KCl, 2 MgCl2, 2 CaCl2, 10 HEPES, and 5 glucose, adjusted to a pH of 7.4 with NaOH and an osmolarity of approximately 318 mOsm using mannitol.

The calcium-free extracellular saline (NO EXT- Ca^{2+}) was formulated with (mM) 140 NaCl, 4 KCl, 4 MgCl2, 10 HEPES, and 0.5 EGTA, also at a pH of 7.4 with NaOH and adjusted to ∼318 mOsm with mannitol.

Stock solutions of 2APB (100 mM) were prepared by dissolving them in methanol and stored at −20 °C.

Statistical Analysis

For calcium imaging in cell cultures, fluorescence time series were manually extracted using both Metamorph (Molecular Devices) and a dynamic-data-exchange Excel file (Microsoft Office 365). Representative traces and statistical analyses of the extracted data from in vitro calcium imaging experiments were conducted with Microcal Origin 8.5 and Prism GraphPad 8.0.2. Bar–dot plots were created using Prism GraphPad 8.0.2. Data comparisons were performed using one-way ANOVA followed by Tukey's multiple comparison test, also utilizing Prism GraphPad 8.0.2. A statistically significant difference was defined as $P \leq 0.05$. All data are presented as mean ± SEM, with the sample size (n) and number of experiments (N) for each statistical analysis indicated in the figure captions corresponding to specific results. The analysis was based on data collected from at least three independent experiments.

■ RESULTS AND DISCUSSION

Substrate Topography and Cell Density Influence Astrocyte Viability and Differentiation

Astrocytes were cultured on three different substrates to evaluate their viability, morphology, and differentiation: Poly-D-lysine (PDL, used as the control) on glass, flat zirconium oxide (flat-ZrOx), and nanostructured zirconium oxide (ns-ZrOx), the latter with a surface roughness of 15 nm. Representative AFM images of the different substrates are reported in Figure 1a. Two seeding densities were employed to assess the effect of cell density on

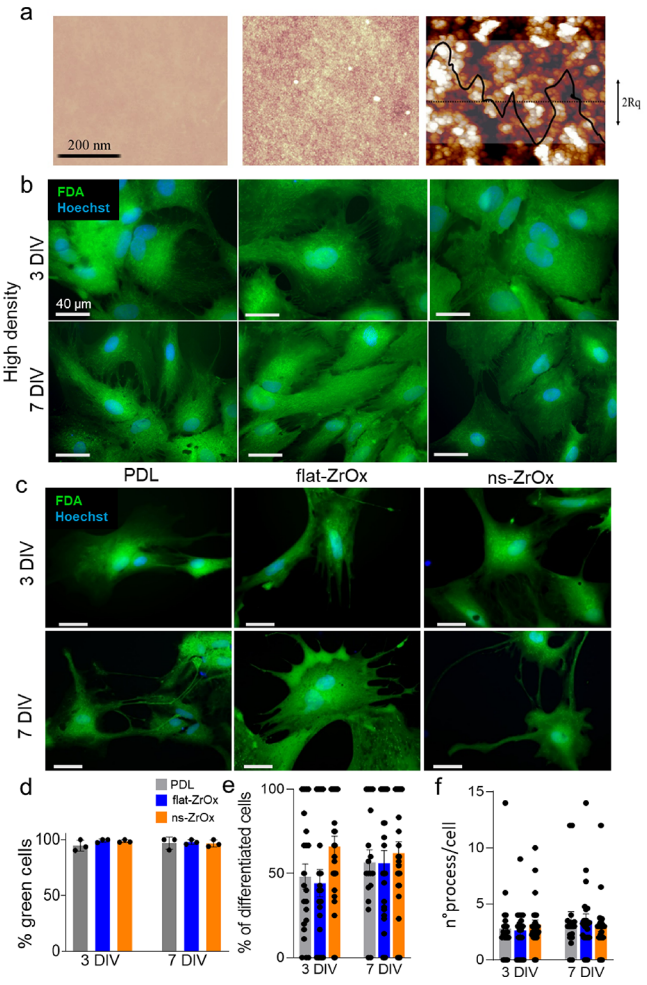

Figure 1. ZrOx substrates support astrocyte viability and morphological differentiation. (a) AFM top-view images of PDL, flat-ZrOx, and nanostructured (ns) ZrOx substrates; Z-bar scale bar ranges from −20 to 20 nm. (b) FDA staining on astrocytes plated on PDL, flat-ZrOx, and ns-ZrOx at 3 and 7 DIV at high density. Note that astrocytes are not differentiated in any of the substrates at any of the time points (scale bar: 40 μm). (c) FDA staining on astrocytes plated on PDL, flat-ZrOx, and ns-ZrOx at 3 and 7 DIV at low density (scale bar: 40 μm). (d) Histogram representing the percentage of green cells (alive cells) plated on PDL at 3 DIV (94.63 ± 2.84, $N = 3$) and 7 DIV (96.88 ± 3.125, $N = 3$), on flat-ZrOx at 3 DIV (99.07 ± 0.92, $N = 3$) and 7 DIV (97.78 ± 1.21, $N = 3$), and on ns-ZrOx at 3 DIV (98.55 ± 0.72, $N = 3$) and 7 DIV (96.56 ± 1.79, $N = 3$). (e) Histogram representing the percentage of differentiated cells in astrocytes plated on PDL at 3 DIV (48.13 ± 7.44, $n = 22$, $N = 3$) and 7 DIV (56.54 ± 7.43, $n = 18$, $N = 3$), on flat-ZrOx at 3 DIV (44.18 ± 8.09, $n = 21$, $N = 3$) and 7 DIV (56.12 ± 7.42, $n = 24$, $N = 3$), and on ns-ZrOx at 3 DIV (65.97 ± 6.19, $n = 26$, $N = 3$) and 7 DIV (62.07 ± 6.72, $n = 25$, $N = 3$). (f) Histogram showing the number of processes per cell in astrocytes plated on PDL at 3 DIV (2.83 ± 0.61, $n = 22$, $N = 3$) and 7 DIV (3.53 ± 0.77, $n = 18$, $N = 3$), on flat-ZrOx at 3 DIV (2.62 ± 0.45, $n = 21$, $N = 3$) and 7 DIV (3.50 ± 0.59, $n = 24$, $N = 3$), and on ns-ZrOx at 3 DIV (3.16 ± 0.41, $n = 26$, $N = 3$) and 7 DIV (3 ± 0.46, $n = 25$, $N = 3$). Data are presented as mean ± SEM. n indicates the number of analyzed cells, and N is the number of independent biological replicates. Statistical significance was assessed by one-way ANOVA followed by Tukey's HSD multiple-comparison test.

https://doi.org/10.1021/acsabm.6c01280
ACS Appl. Bio Mater. 2026, 9, 8345−8358

astrocyte behavior: high density (30,000 cells) and low density (15,000 cells). Cell viability and morphology were analyzed using FDA staining, providing key insights into how substrate type and cell density influence astrocyte responses over time.

FDA staining showed that astrocytes plated at both densities demonstrated consistent viability across all substrates, as evidenced by the presence of viable cells (green cells) at both 3 and 7 DIV (Figure 1b,c).

From a morphological point of view, the cells plated at high density appeared polygonal and did not show the presence of processes (Figure 1b), whereas astrocytes cultured at low density exhibited a pronounced increase in differentiation, as demonstrated by the formation of processes extending from the soma on all substrates (Figure 1c).

Quantitative analysis revealed no significant differences in cell adhesion or viability among the three substrates as the percentage of viable (green-stained) astrocytes was comparable between the control substrate [PDL (3 DIV: 94.63 ± 2.84, $N = 3$; 7 DIV: 96.88 ± 3.125, $N = 3$)] and the ZrOx substrates [flat-ZrOx (3 DIV: 99.07 ± 0.92, $N = 3$; 7 DIV: 97.78 ± 1.21, $N = 3$) and ns-ZrOx (3 DIV: 98.55 ± 0.72, $N = 3$; 7 DIV: 96.56 ± 1.79, $N = 3$)] (Figure 1d). At low cell density, the proportion of differentiated astrocytes showed a slight, although not statistically significant, increase on ns-ZrOx compared to PDL at both time points [PDL (3 DIV: 48.13 ± 7.44, $n = 22$, $N = 3$; 7 DIV: 56.54 ± 7.43, $n = 18$, $N = 3$), flat-ZrOx (3 DIV: 44.18 ± 8.09, $n = 21$, $N = 3$; 7 DIV: 56.12 ± 7.42, $n = 24$, $N = 3$), and ns-ZrOx (3 DIV: 65.97 ± 6.19, $n = 26$, $N = 3$; 7 DIV: 62.07 ± 6.72, $n = 25$, $N = 3$)] (Figure 1e). In contrast, no differences were observed among substrates in the number of cellular processes per cell [PDL (3 DIV: 2.83 ± 0.61, $n = 22$, $N = 3$; 7 DIV: 3.53 ± 0.77, $n = 18$, $N = 3$), flat-ZrOx (3 DIV: 2.62 ± 0.45, $n = 21$, $N = 3$; 7 DIV: 3.50 ± 0.59, $n = 24$, $N = 3$), and ns-ZrOx (3 DIV: 3.16 ± 0.41, $n = 26$, $N = 3$; 7 DIV: 3 ± 0.46, $n = 25$, $N = 3$)] (Figure 1f).

Collectively, these data indicate that from a morphological standpoint, either astrocyte plated on PDL and on ZrOx substrates at high density maintained an undifferentiated state, with an almost complete absence of differentiated cells at both time points (data not shown). This suggests that high-density conditions may inhibit the initiation of differentiation, potentially due to limited space for cell extension or altered intercellular signaling in crowded environments.[28]

The reduced cell–cell contact, and increased availability of substrate surface may promote signaling pathways and cytoskeletal remodeling necessary for process extension and maturation. The results suggest that substrate chemistry by itself does not significantly alter astrocyte viability but may interact with cell density to influence differentiation. Specifically, while flat-ZrOx and ns-ZrOx supported similar viability to the control, the low-density seeded cell condition appeared more permissive for differentiation across all substrates. These findings are in agreement with previous reports indicating that cell seeding density modulates cell morphology and functional state,[29,30] providing valuable insights for biomaterial development and neural tissue engineering applications. Substrate topography is well known to influence key cellular processes, including migration, adhesion, and polarization; in stem cells, it has also been shown to play a crucial role in guiding differentiation.[31,32] Similarly, studies on primary astrocytes have demonstrated that nanostructured surfaces can enhance their differentiation rate.[33,34] Astrocyte differentiation on nanostructured surfaces is frequently accompanied by an increase in calcium signaling.[35] Activation of calcium-dependent signaling pathways, such as RHO, TGF-β, or FAK, can drive cells toward distinct differentiation states;[36–38] notably, these pathways are tightly interconnected with canonical mechanotransduction mechanisms, which are themselves responsive to substrate nanotopography.[31]

Substrate Nanotopography Differentially Modulates Intracellular Calcium Signaling Pathways in Astrocytes

Given the importance of calcium signaling on astrocytes and the functional response of astrocytes to different substrates, we performed calcium imaging on cells cultured on PDL, flat-ZrOx, and ns-ZrOx. This analysis revealed significant differences in intracellular calcium ($[Ca^{2+}]_i$) dynamics between the control and ZrOx substrates, highlighting the influence of substrate material and structure on astrocyte behavior.

Figure 2b shows the temporal changes in calcium intensity, revealing substrate-driven calcium dynamics. Astrocytes cultured on ns-ZrOx exhibited a markedly stronger maximal calcium amplitude ($\Delta F/F$) (0.30 ± 0.036, $n = 55$, $N = 10$) compared to those on the control substrate (0.19 ± 0.016, $n = 78$, $N = 10$) (Figure 2c), accompanied by a significantly shorter time onset (ns-ZrOx: 111.1 ± 9.49, $n = 55$, $N = 10$; PDL: 166.5 ± 8.47, $n = 78$, $N = 10$) (Figure 2d) and time to peak (ns-ZrOx: 213 ± 10.84, $n = 55$, $N = 10$; PDL: 247.6 ± 5.53, $n = 78$, $N = 10$) (Figure 2e).

These findings indicate that the nanostructured surface not only amplified the calcium response but also accelerated its kinetics, suggesting a more rapid and intense cellular activation. Similarly, astrocytes on flat-ZrOx displayed a significantly shorter time onset (120.7 ± 8.75, $n = 68$, $N = 10$) compared to the control substrate, although the differences on maximal amplitude (0.26 ± 0.029, $n = 68$, $N = 10$) and time to peak (226.8 ± 8.71, $n = 68$, $N = 10$) were less pronounced than on ns-ZrOx.

Interestingly, the number of calcium peaks, indicative of the frequency of calcium oscillations, did not differ significantly across the three substrates (PDL: 1.88 ± 0.13, $n = 78$, $N = 10$; flat-ZrOx: 2.36 ± 0.22, $n = 68$, $N = 10$; ns-ZrOx: 2.45 ± 0.26, $n = 55$, $N = 10$) (Figure 2f). This suggests that while the material and nanostructured surface modulate the intensity and speed of calcium signaling, they do not alter the overall pattern of calcium dynamics. These results demonstrate that substrate chemistry does not affect cell viability; however, substrate chemical composition and topography directly influence the functionality of astrocytes, namely, their calcium signaling. Specifically, the ns-ZrOx surface enhances both the amplitude and shorten the onset of the calcium response, suggesting that nanoscale features may optimize substrate–cell interactions, potentially by affecting ion channel activity, receptor clustering, or mechanosensitive pathways. These findings provide valuable insights into how material morphology can be leveraged to modulate astrocyte function, with implications for biomaterial development and neural tissue engineering.

We next applied selective pharmacological approaches to investigate the contribution of calcium influx and internal stores to the substrate-dependent differences in astrocytes' calcium signaling.

2-Aminoethyl diphenylborinate (2APB), a cell-permeable inhibitor of inositol 1,4,5-trisphosphate ($Ins(1,4,5)P_3$ or IP_3)-induced Ca^{2+} release, was used to assess the role of IP_3 signaling in astrocyte calcium dynamics across different substrates.

https://doi.org/10.1021/acsabm.6c01280
ACS Appl. Bio Mater. 2026, 9, 8345–8358

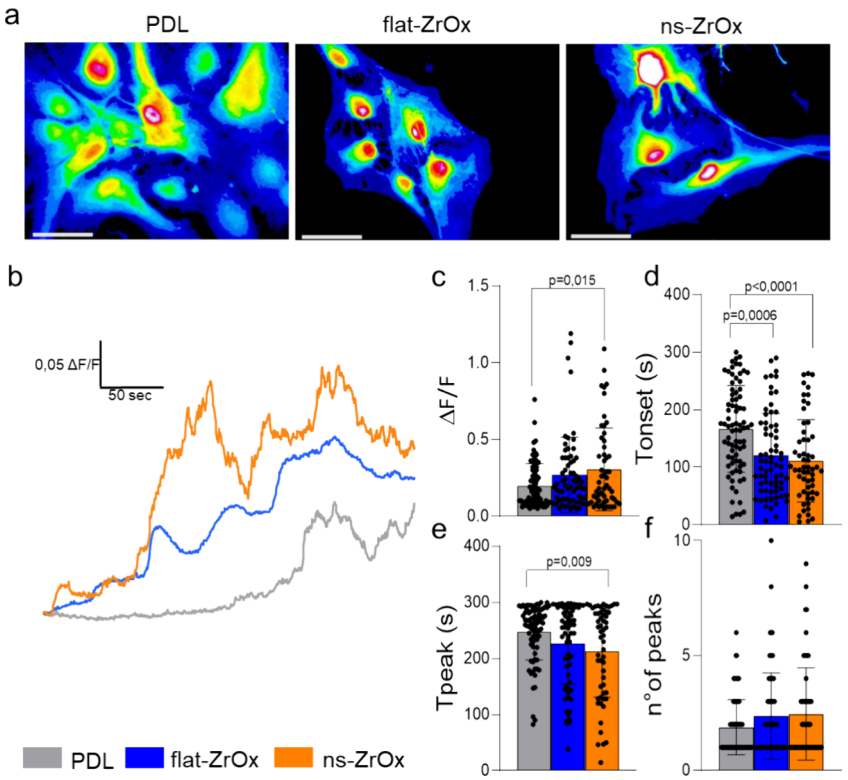

Figure 2. ZrOx modulates spontaneous calcium dynamics in astrocytes. (a) Representative images illustrating the spatial distribution of calcium waves in astrocytes grown on PDL, flat-ZrOx, and ns-ZrOx surfaces (scale bar: 40 μm). (b) Representative traces of fluorescence intensity variation ($\Delta F/F$) over time of the astrocytes plated on the different substrates. (c) Histogram showing maximum fluorescence intensity values in responding astrocytes cultured on PDL (0.19 ± 0.016, $n = 78$, $N = 10$), flat-ZrOx (0.26 ± 0.029, $n = 68$, $N = 10$), and ns-ZrOx (0.30 ± 0.036, $n = 55$, $N = 10$). Astrocytes on PDL showed significantly lower maximum fluorescence intensity compared to ns-ZrOx ($^{*}p = 0.015$). (d) Histogram showing the time onset in responding astrocytes cultured on PDL (166.5 ± 8.47, $n = 78$, $N = 10$), flat-ZrOx (120.7 ± 8.75, $n = 68$, $N = 10$), and ns-ZrOx (111.1 ± 9.49, $n = 55$, $N = 10$). Astrocytes on PDL showed significantly slower response compared to flat-ZrOx ($^{***}p = 0.0006$) and ns-ZrOx ($^{****}p < 0.0001$). (e) Histogram showing the time to peak in responding astrocytes cultured on PDL (247.6 ± 5.53, $n = 78$, $N = 10$), flat-ZrOx (226.8 ± 8.71, $n = 68$, $N = 10$), and ns-ZrOx (213 ± 10.84, $n = 55$, $N = 10$). Astrocytes on PDL showed significantly slower time to peak compared to ns-ZrOx ($^{**}p = 0.009$). (f) Histogram showing the number of peaks in responding astrocytes cultured on PDL (1.88 ± 0.13, $n = 78$, $N = 10$), flat-ZrOx (2.36 ± 0.22, $n = 68$, $N = 10$), and ns-ZrOx (2.45 ± 0.26, $n = 55$, $N = 10$).

The calcium-free extracellular saline ($0Ca^{2+}$) was employed to eliminate extracellular calcium flux, thereby enabling the exclusive observation of intracellular calcium dynamics. This approach isolates the contributions of internal calcium stores and pathways, providing a clearer understanding of intracellular calcium signaling mechanisms.

Figure 3a shows representative calcium traces in astrocytes cultured on distinct substrates, following both IP_3-dependent signaling inhibition and extracellular calcium removal.

The data illustrated in Figure 3 reveal significant alterations in astrocyte calcium activity upon 2APB treatment, particularly for cells cultured on ns-ZrOx. Astrocytes on ns-ZrOx exhibited a pronounced reduction in maximal calcium amplitude ($\Delta F/F$) (ns-ZrOx: 0.099 ± 0.016, $n = 15$, $N = 3$) (Figure 3b), indicating diminished release from intracellular calcium stores. Additionally, the time onset of calcium transients was significantly increased (ns-ZrOx: 170.9 ± 18.43, $n = 15$, $N = 3$), demonstrating a delay in the initiation of calcium signaling.

These findings suggest that the nanostructured surface amplifies IP_3-dependent calcium signaling under normal conditions, making it particularly susceptible to disruption by 2APB. The observed changes were less evident on other substrates, underscoring the unique influence of the ns-ZrOx surface on IP_3-mediated calcium dynamics.

Interestingly, the removal of extracellular Ca^{2+} did not affect the maximal calcium amplitude ($\Delta F/F$) in ZrOx (flat-ZrOx: 0.21 ± 0.034, $n = 32$, $N = 3$; ns-ZrOx 0.36 ± 0.1, $n = 11$, $N = 3$) (Figure 3b), as the values remained comparable to those observed under normal conditions. However, the absence of extracellular calcium significantly influenced other critical aspects of calcium signaling. The time to onset of the calcium response was markedly prolonged (PDL: 197.2 ± 9.83, $n = 9$, $N = 3$; flat-ZrOx: 194.3 ± 10.83, $n = 32$, $N = 3$; ns-ZrOx 184.1 ± 12.44, $n = 11$, $N = 3$) (Figure 3c), indicating that extracellular calcium may play a role in accelerating the initiation of intracellular calcium release. Additionally, the number of calcium peaks was reduced on ZrOx substrates, significantly on flat-ZrOx (flat-ZrOx: 1.31 ± 0.12, $n = 32$, $N = 3$; ns-ZrOx: 1.36 ± 0.15, $n = 11$, $N = 3$) (Figure 3e), suggesting that extracellular calcium contributes to the frequency modulation of calcium transients. These findings imply that while the magnitude of calcium signaling can be sustained through intracellular stores, extracellular calcium is essential for fine-tuning the temporal and dynamic features of calcium signaling pathways.

https://doi.org/10.1021/acsabm.6c01280
ACS Appl. Bio Mater. 2026, 9, 8345−8358

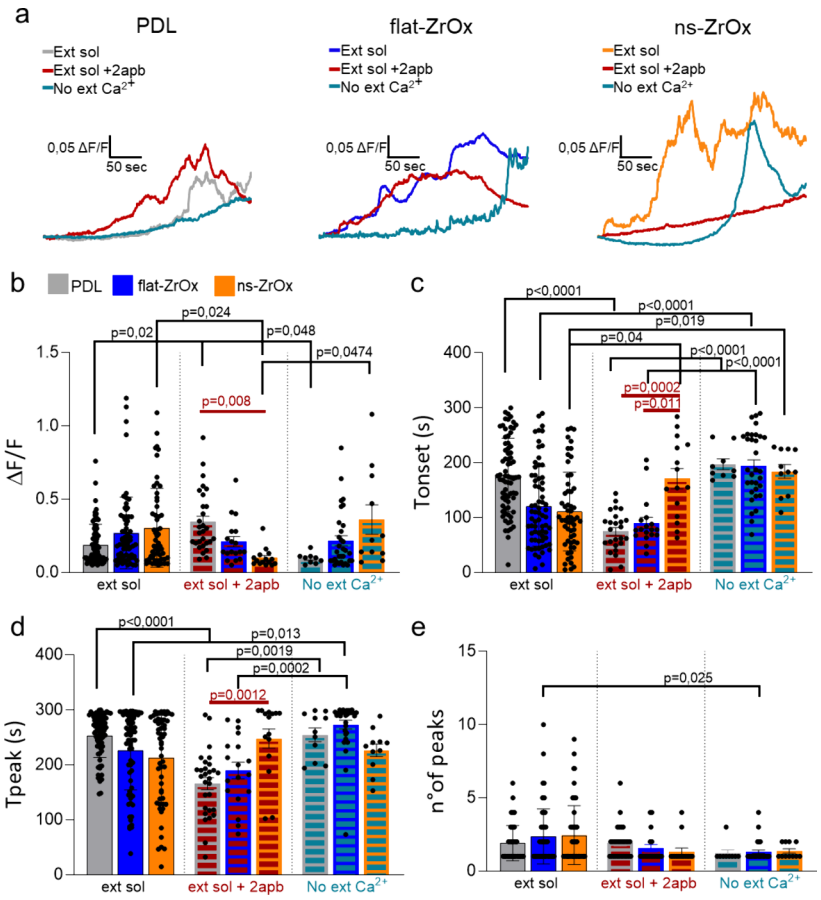

Figure 3. Astrocyte calcium signaling on ZrOx depends on both intracellular release and extracellular Ca^{2+} entry. (a) Representative traces showing $\Delta F/F$ fluorescence intensity changes over time in astrocytes on all substrates, comparing control conditions with IP_3 pathway inhibition and removal of external Ca^{2+}. (b) Histogram showing maximum fluorescence intensity values in responding astrocytes cultured on PDL, flat-ZrOx, and ns-ZrOx in control conditions, following IP_3 pathway inhibition [Ext sol + 2apb: PDL (0.34 ± 0.038, $n = 29$, $N = 3$), flat-ZrOx (0.20 ± 0.034, $n = 18$, $N = 3$), and ns-ZrOx (0.099 ± 0.016, $n = 15$, $N = 3$)], and removal of external Ca^{2+} [No ext Ca^{2+}: PDL (0.09 ± 0.011, $n = 9$, $N = 3$), flat-ZrOx (0.21 ± 0.034, $n = 32$, $N = 3$), and ns-ZrOx (0.36 ± 0.1, $n = 11$, $N = 3$)]. (c) Histogram showing the time onset in responding astrocytes cultured on PDL, flat-ZrOx, and ns-ZrOx in control conditions, following IP_3 pathway inhibition [Ext sol + 2apb: PDL (74.62 ± 7.25, $n = 29$, $N = 3$), flat-ZrOx (90.06 ± 10.30, $n = 18$, $N = 3$), and ns-ZrOx (170.9 ± 18.43, $n = 15$, $N = 3$)], and removal of external Ca^{2+} [No ext Ca^{2+}: PDL (197.2 ± 9.83, $n = 9$, $N = 3$), flat-ZrOx (194.3 ± 10.83, $n = 32$, $N = 3$), and ns-ZrOx (184.1 ± 12.44, $n = 11$, $N = 3$)]. (d) Histogram showing the time to peak in responding astrocytes cultured on PDL, flat-ZrOx, and ns-ZrOx in control conditions, following IP_3 pathway inhibition [Ext sol + 2apb: PDL (165.8 ± 10.94, $n = 29$, $N = 3$), flat-ZrOx (189.5 ± 15.11, $n = 18$, $N = 3$), and ns-ZrOx (247.9 ± 17.47, $n = 15$, $N = 3$)], and removal of external Ca^{2+} [No ext Ca^{2+}: PDL (254.7 ± 12.49, $n = 9$, $N = 3$), flat-ZrOx (273.3 ± 7.99, $n = 32$, $N = 3$), and ns-ZrOx (226.3 ± 11.75, $n = 11$, $N = 3$)]. (e) Histogram showing the number of peaks in responding astrocytes cultured on PDL, flat-ZrOx, and ns-ZrOx in control conditions, following IP_3 pathway inhibition [Ext sol + 2apb: PDL (1.93 ± 0.21, $n = 29$, $N = 3$), flat-ZrOx (1.55 ± 0.24, $n = 18$, $N = 3$), and ns-ZrOx (1.33 ± 0.23, $n = 15$, $N = 3$)], and removal of external Ca^{2+} [No ext Ca^{2+}: PDL (1.22 ± 0.22, $n = 9$, $N = 3$), flat-ZrOx (1.31 ± 0.12, $n = 32$, $N = 3$), and ns-ZrOx (1.36 ± 0.15, $n = 11$, $N = 3$)]. p values are displayed on the figure.

The ability of ns-ZrOx to amplify intracellular calcium responses suggests that the nanostructured interface enhances the mechanosensitivity of astrocyte membranes, possibly by reorganizing integrin clusters, focal adhesions, or associated ion channels such as TRP or Piezo family members.[39,40]

The application of 2APB, an IP_3 receptor antagonist, revealed that the enhanced calcium signaling on ns-ZrOx is strongly dependent on IP_3-mediated intracellular calcium release. The pronounced sensitivity of astrocytes to IP_3R inhibition on the nanostructured surface indicates that the substrate actively promotes ER–plasma membrane communication or potentiates phosphoinositide signaling pathways.[1,41] Interestingly, in calcium-free conditions, astrocytes maintained similar signal amplitudes but displayed delayed response kinetics and reduced oscillation frequency, supporting the hypothesis that extracellular calcium influx contributes primarily to the temporal modulation rather than the magnitude of intracellular calcium dynamics.

Zirconia-Based Substrates Demonstrate High Biocompatibility with DRG Neuron–Glia Co-Cultures and Drive Their Functional Behavior

To extend our investigation of zirconia-based substrates beyond the central nervous system (CNS) and into the peripheral nervous system (PNS), we established a co-culture model of DRG neurons and glial cells. DRG cultures represent a well-established and physiologically relevant system for studying peripheral sensory neurons and their interactions with associated glia, and they serve as a powerful in vitro model to explore

https://doi.org/10.1021/acsabm.6c01280
ACS Appl. Bio Mater. 2026, 9, 8345−8358

sensory system development, injury responses, and neuroregenerative mechanisms.[42]

As illustrated in Figure 4a,b, all tested ZrOx substrates exhibited excellent biocompatibility with DRG co-cultures. FDA images show the presence of green (alive) cells with different morphological features (Figure 4a). The quantitative analysis of cell survival indicates no significant impairment of cell adhesion across the groups (PDL: 95.70 ± 2.22; flat-ZrOx: 99.37 ± 0.46; ns-ZrOx: 98.12 ± 1.22) (Figure 4b). Importantly, DRG neurons can be clearly identified by their characteristic spherical or ovoid somata, often grouped in clusters, which is consistent with their native morphology in vivo.

This neuronal identity was further validated through immunocytochemical staining for growth-associated protein-43 (GAP-43), a well-established marker of axonal growth and regeneration that is particularly prominent in developing or regenerating DRG neurons (Figure 4c).[43]

The glial cells, which surround and support the neurons in culture, also showed typical elongated morphologies and close association with neuronal somata and neurites, consistent with functional neuron–glia interactions. Together, these results confirm that zirconia substrates support healthy co-culture conditions for DRG-derived cells, validating their applicability in PNS-targeted neuroengineering approaches and supporting their potential use in biointerfaces for peripheral nerve repair or stimulation.

To investigate how the substrate morphology and chemistry influence cellular excitability and signaling, we performed a detailed analysis of calcium dynamics in DRG co-cultures seeded on the three different substrates. Calcium transients were recorded in both neuronal and glial populations under the previous distinct conditions: (1) control physiological solution, (2) following 2APB administration, and (3) in calcium-free extracellular medium. Figure 5 presents calcium responses of DRG neurons and glial cells on three different substrates under control conditions. Representative traces in Figure 5b reveal the substrate-specific temporal dynamics of calcium signaling in both cell types. Notably, glial cells on ns-ZrOx (0.34 ± 0.028, $n = 97$, $N = 10$) showed significantly higher $\Delta F/F$ amplitudes compared to those cultured on PDL (0.23 ± 0.023, $n = 83$, $N = 10$) (Figure 5c), suggesting that zirconia substrates enhance glial responsiveness. Among the zirconia variants, DRG glial cells plated on ns-ZrOx showed a tendency toward faster onset (flat-ZrOx: 103.2 ± 6.15, $n = 68$, $N = 10$; ns-ZrOx: 85.46 ± 5.83, $n = 97$, $N = 10$) (Figure 5d), indicating more rapid calcium entry and/or mobilization from intracellular stores. This accelerated response may reflect enhanced mechanosensitivity or improved interface-mediated signaling due to the nanoscale topography, while we do not observe any difference in the time to peak and the number of peaks in glial calcium signaling among the substrates (Figure 5e,f)

In neurons, cultures on ns-ZrOx exhibited a trend toward stronger calcium responses, although differences in $\Delta F/F$ amplitude across substrates did not reach statistical significance (Figure 5c). Nevertheless, the consistently higher baseline activity (0.41 ± 0.06, $n = 22$, $N = 10$) and shorter time of onset (64.21 ± 12.6, $n = 21$, $N = 10$) observed on ns-ZrOx relative to flat-ZrOx ($\Delta F/F$ amplitude: 0.37 ± 0.12, $n = 9$, $N = 10$; time onset: 143.4 ± 32.2, $n = 9$, $N = 10$) support the hypothesis that nanostructuring enhances neuronal excitability or responsiveness (Figure 5c,d). While analyzing the time to peak, we did not find any significant difference among the groups. [PDL

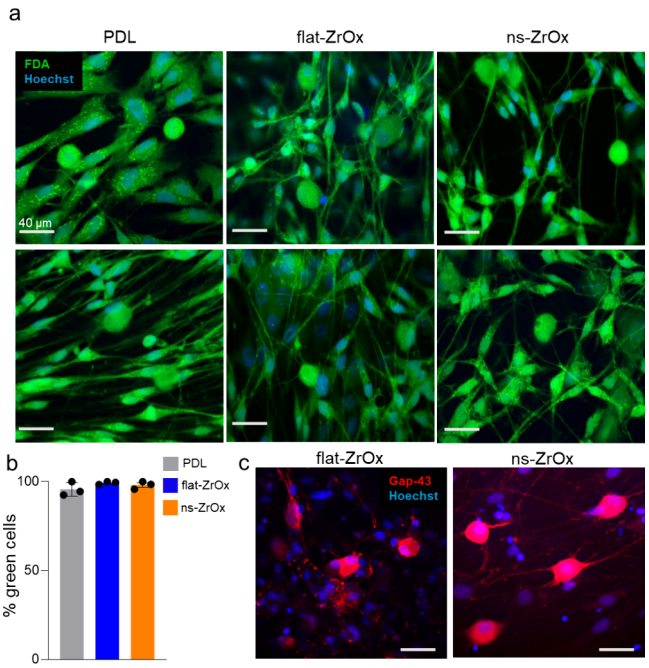

Figure 4. ZrOx support DRG neuron–glia viability. (a) FDA staining of DRG neuron–glia co-cultures plated on PDL, flat-ZrOx, and ns-ZrOx substrates at 5 DIV (scale bar: 40 μm). (b) Histogram showing the percentage of viable (green) cells on PDL (95.70 ± 2.22, $N = 3$), flat-ZrOx (99.37 ± 0.46, $N = 3$), and ns-ZrOx (98.12 ± 1.22, $N = 3$). (c) Immunofluorescence images of GAP-43–positive cells. Rounded GAP-43–positive cells are likely neurons (scale bar: 40 μm).

(234.2 ± 17.08, $n = 14$, $N = 10$), flat-ZrOx (280.8 ± 5.56, $n = 9$, $N = 10$), and ZrOx (252.5 ± 12.47, $n = 21$, $N = 10$)] (Figure 5e). The number of peaks was similar across the groups [PDL (glia: 1.27 ± 0.06, $n = 83$; neuron: 1.35 ± 0.24, $n = 14$, $N = 10$), flat-ZrOx (glia: 1.34 ± 0.075, $n = 68$, $N = 10$; neuron: 1 ± 0, $n = 9$, $N = 10$), and ns-ZrOx (glia: 1.24 ± 0.04, $n = 97$; neuron: 1.35 ± 0.15, $n = 21$, $N = 10$)] (Figure 5f). These results suggest that ns-ZrOx not only supports robust cell viability but also actively modulates functional calcium signaling, especially in glial populations.

Given the central role of calcium in neuron–glia communication and plasticity, these findings underscore the glio-neuromorphic potential of ns-ZrOx substrates. Figure 6 shows the percentage of responsive DRG neurons and glia plated on the three substrates in control conditions and following the treatment with 2APB and in the absence of extracellular calcium.

Following the treatment with 2APB, we observed distinct substrate-dependent alterations in calcium signaling within both neuronal and glial populations of the DRG co-cultures. Specifically, neuronal calcium activity was completely abolished on PDL (Figure 6a) and flat-ZrOx (Figure 6b), whereas ns-ZrOx (23.06 ± 11%; $N = 4$) (Figure 6c) preserved residual calcium signaling, indicating a partial resistance to IP_3R inhibition or the possible contribution of alternative calcium sources, such as mechanosensitive pathways supported by the nanostructured interface.

Glial cells in the DRG preparation exhibited a significant reduction in the percentage of responding cells across all substrates (PDL: 1.67 ± 1.67%, $N = 10$; flat-ZrOx: 18 ± 6.23%, $N = 10$; ns-ZrOx: 8.53 ± 2.86%) following 2APB treatment, with respect to control conditions (PDL: 63.23 ±

https://doi.org/10.1021/acsabm.6c01280
ACS Appl. Bio Mater. 2026, 9, 8345−8358

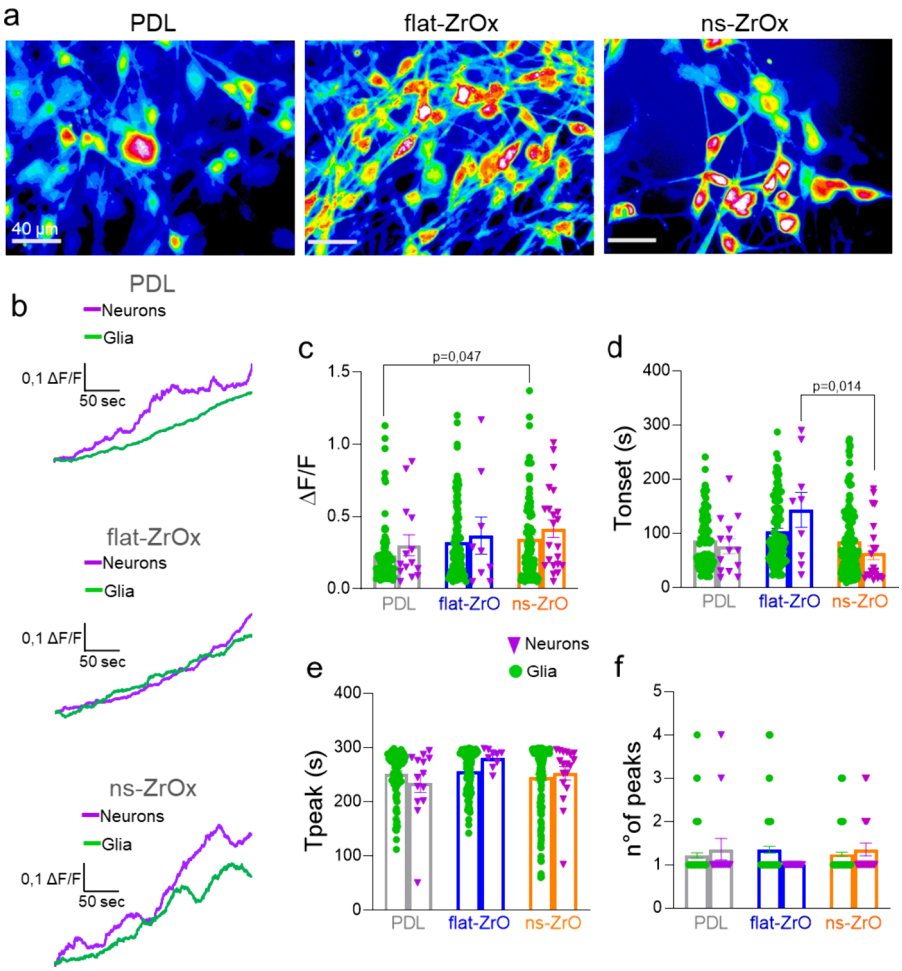

Figure 5. ZrOx enhances calcium signaling in DRG neuron–glia co-cultures. (a) Representative images illustrating the spatial distribution of calcium waves in DRG neuron–glia co-cultures grown on PDL, flat-ZrOx, and ns-ZrOx surfaces (scale bar: 40 μm). (b) Representative traces of fluorescence intensity variation ($\Delta F/F$) over time of DRG neuron and glia plated on all the substrates. (c) Histogram showing maximum fluorescence intensity values in responding astrocytes cultured on PDL (glia: 0.23 ± 0.023, $n = 83$; neuron: 0.30 ± 0.07, $n = 14$, $N = 10$), flat-ZrOx (glia: 0.32 ± 0.026, $n = 68$; neuron: 0.37 ± 0.12, $n = 9$, $N = 10$), and ns-ZrOx (glia: 0.34 ± 0.028, $n = 97$; neuron: 0.41 ± 0.06, $n = 22$, $N = 10$). (d) Histogram showing the time onset in responding DRG neuron and glia cultured on PDL (glia: 87.15 ± 5.63, $n = 83$; neuron: 76.32 ± 13.91, $n = 14$, $N = 10$), flat-ZrOx (glia: 103.2 ± 6.15, $n = 68$, $N = 10$; neuron: 143.4 ± 32.2, $n = 9$, $N = 10$), and ns-ZrOx (glia: 85.46 ± 5.83, $n = 97$; neuron: 64.21 ± 12.6, $n = 21$, $N = 10$). (e) Histogram showing the time to peak in responding DRG neurons and glia cultured on PDL (glia: 251.9 ± 4.90, $n = 83$; neuron: 234.2 ± 17.08, $n = 14$, $N = 10$), flat-ZrOx (glia: 256 ± 3.91, $n = 68$, $N = 10$; neuron: 280.8 ± 5.56, $n = 9$, $N = 10$), and ns-ZrOx (glia: 244.8 ± 5.42, $n = 97$; neuron: 252.5 ± 12.47, $n = 21$, $N = 10$). (f) Histogram showing the number of peaks in responding DRG neurons and glia cultured on PDL (glia: 1.27 ± 0.06, $n = 83$; neuron: 1.35 ± 0.24, $n = 14$, $N = 10$), flat-ZrOx (glia: 1.34 ± 0.075, $n = 68$, $N = 10$; neuron: 1 ± 0, $n = 9$, $N = 10$), and ns-ZrOx (glia: 1.24 ± 0.04, $n = 97$; neuron: 1.35 ± 0.15, $n = 21$, $N = 10$). p values are displayed on the figure.

13.34% $N = 10$; flat-ZrOx: 65.23 ± 11.38%, $N = 10$; ns-ZrOx: 74.77 ± 9.14%, $N = 10$), suggesting a strong dependence on IP_3R-mediated signaling. Whereas in the absence of calcium in the extracellular solution, a good percentage of both glial and neuronal cells maintained the activity [PDL (glia: 35.21 ± 21.35%; neurons: 25 ± 25%; $N = 4$), flat-ZrOx: (glia: 49.66 ± 16.59%; neurons: 47.92 ± 22.15%; $N = 4$), and ns-ZrOx (glia: 59.95 ± 17.25%; neurons: 34.43 ± 15.20%; $N = 4$)] (Figure 6).

As shown in Figure 7, inhibition of IP_3 signaling and depletion of extracellular calcium significantly alter calcium dynamics in glial cells across all three substrates.

Following IP_3R blockage, we observed that on ns-ZrOx, the $\Delta F/F$ amplitude in glial cells was significantly reduced (0.10 ± 0.012, $n = 11$, $N = 3$) (Figure 7b), the time of onset was markedly increased (156.4 ± 23.49, $n = 11$, $N = 3$) (Figure 7c), while time to peak (225.7 ± 25.54, $n = 11$, $N = 3$) (Figure 7d) and number of peaks (1.27 ± 0.14, $n = 11$, $N = 3$) (Figure 7e) did not differ from the control media. A similar trend was observed on flat-ZrOx, where glial responses were also diminished in both amplitude (0.14 ± 0.014, $n = 33$, $N = 3$) (Figure 7b) and temporal kinetics (158.9 ± 9.53, $n = 33$, $N = 3$) (Figure 7c).

Interestingly, glial cells cultured on PDL did not exhibit a statistically significant reduction in calcium response amplitude (0.11 ± 0.04, $n = 3$, $N = 3$) or in response timing (78 ± 37.80, $n = 3$, $N = 3$) following 2APB treatment, suggesting that calcium dynamics on this conventional substrate may involve additional or compensatory mechanisms, or reflect lower basal IP_3R engagement.

Across all conditions and substrates, both the time of onset and the time to peak of calcium transients were increased

https://doi.org/10.1021/acsabm.6c01280
ACS Appl. Bio Mater. 2026, 9, 8345−8358

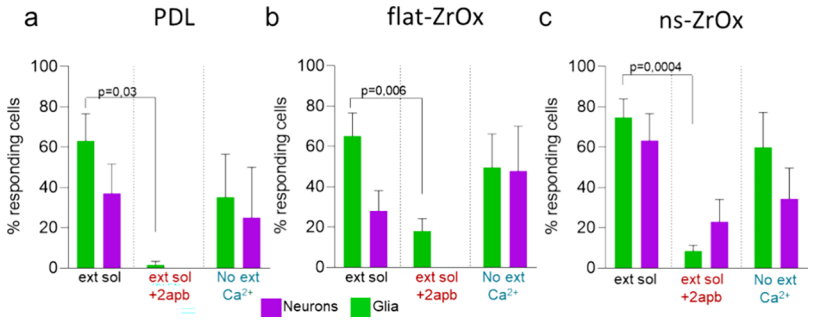

Figure 6. Modulation of DRG neuron and glia responsiveness by internal and external calcium pathways. (a) Histogram showing the percentage of responding DRG neurons and glial cells cultured on PDL under different experimental conditions. Data are presented as mean ± SEM for control (glia: 63.23 ± 13.34%; neurons: 37.04 ± 14.7%; $N = 10$), following 2APB treatment (glia: 1.67 ± 1.67%; neurons: 0 ± 0%; $N = 4$), and after extracellular calcium depletion (glia: 35.21 ± 21.35%; neurons: 25 ± 25%; $N = 4$). (b) Histogram showing the percentage of responding DRG neurons and glial cells cultured on flat-ZrOx under different experimental conditions. Data are presented as mean ± SEM for control (glia: 65.23 ± 11.38%; neurons: 28.00 ± 10.6%; $N = 10$), following 2APB treatment (glia: 18 ± 6.23%; neurons: 0 ± 0%; $N = 4$), and after extracellular calcium depletion (glia: 49.66 ± 16.59%; neurons: 47.92 ± 22.15%; $N = 4$). (c) Histogram showing the percentage of responding DRG neurons and glial cells cultured on ns-ZrOx under different experimental conditions. Data are presented as mean ± SEM for control (glia: 74.77 ± 9.14%; neurons: 63.33 ± 13.33%; $N = 10$), following 2APB treatment (glia: 8.53 ± 2.86%; neurons: 23.06 ± 11%; $N = 4$), and after extracellular calcium depletion (glia: 59.95 ± 17.25%; neurons: 34.43 ± 15.20%; $N = 4$). p values are displayed on the figure.

following 2APB administration, with the most pronounced delays observed on ns-ZrOx (Figure7). These findings highlight a substrate-specific modulation of intracellular calcium signaling pathways and further reinforce the notion that ns-ZrOx differentially interfaces with glial and neuronal physiology.

In the absence of extracellular calcium, we observed substrate-dependent alterations in intracellular calcium dynamics within both glial cells and neurons cultured on ZrOx substrates. Glial cells plated on ns-ZrOx exhibited a tendency toward the reduction in the $\Delta F/F$ amplitude (0.22 ± 0.03, $n = 41$, $N = 3$) (Figure 7b), accompanied by a significant increase in the time of onset (157.5 ± 9.58, $n = 42$, $N = 3$) (Figure 7c) and a slight increase of the time to peak (267.7 ± 5.31, $n = 41$, $N = 3$) of the calcium transient (Figure 7d). These findings indicate a strong dependence on extracellular calcium influx for initiating and shaping calcium signals in glia on ns-ZrOx, possibly due to enhanced membrane interaction or modulation of mechanosensitive or store-operated calcium channels by the nanostructured surface.

Conversely, glial cells on flat-ZrOx maintained a preserved $\Delta F/F$ amplitude (0.24 ± 0.045, $n = 27$, $N = 3$) (Figure 7b), and notably, the time to peak was slightly shorter (232.1 ± 13.34, $n = 27$, $N = 3$) (Figure 7d), suggesting a more stable or sustained reliance on intracellular calcium stores and potentially a reduced sensitivity to the removal of extracellular calcium.

In Figure 8 we show the properties of neuronal calcium dynamics plated on all the substrates.

Following extracellular Ca^{2+} removal, only two neurons remained responsive on PDL, while no responding neurons were detected after IP_3 pathway inhibition on either PDL or flat-ZrOx. Consequently, quantitative analyses of calcium signaling parameters were not performed for these conditions because the number of responding cells was insufficient for meaningful statistical analysis.

In the neuronal population, the magnitude of the calcium response ($\Delta F/F$) after extracellular calcium removal was significantly reduced across both zirconia substrates (flat-ZrOx: 0.18 ± 0.040, $n = 7$, $N = 3$; ns-ZrOx: 0.23 ± 0.08, $n = 6$, $N = 3$) (Figure 8b), indicating a critical role of extracellular calcium influx in neuronal calcium signaling regardless of surface topography. Following IP_3 pathway inhibition, a significant reduction in $\Delta F/F$ was observed in neurons cultured on ns-ZrOx (0.23 ± 0.04, $n = 9$, $N = 3$), indicating that spontaneous calcium activity on the nanostructured substrate is also dependent on intracellular calcium release. Only neurons on ns-ZrOx exhibited a significantly delayed time of onset in extracellular calcium absence (159.8 ± 24.8, $n = 6$, $N = 3$) and following IP_3 pathway inhibition (190.5 ± 21.43, $n = 9$, $N = 3$) (Figure 8c), suggesting that nanostructuring the surface may affect the kinetics of calcium mobilization, possibly by altering membrane potential, receptor distribution, or the availability of residual intracellular stores. Time to peak and number of peaks remained unchanged in all the zirconia substrates at all conditions (Figure 8d,e).

These data highlight that surface nanotopography modulates not only the amplitude of calcium responses but also their temporal features, in a cell-type-specific manner, reinforcing the potential of ns-ZrOx as a functional interface for glio-neuromorphic applications.

DISCUSSION

The present study demonstrates that ns-ZrOx films are a biocompatible and functionally active interface for both astrocytes and peripheral neuron–glia co-cultures. By comparing cellular behavior on nanostructured vs flat-ZrOx substrates, we show that nanoscale topography not only supports cell survival and differentiation but also modulates the amplitude and temporal dynamics of calcium signaling. These effects are consistent across both central (astrocytes) and peripheral (DRG) glial populations, highlighting the potential of ns-ZrOx as a versatile neurogliomorphic material capable of promoting and modulating neuroglial communication.

Astrocytes cultured on ZrOx substrates, both nanostructured and flat, displayed enhanced calcium signaling compared to cells grown on PDL-coated substrates. This enhancement was characterized by statistically significant increased calcium transient amplitude and faster response kinetics. Notably, astrocytes plated on ns-ZrOx exhibited a further potentiation of these effects, indicating that the nanostructured topography amplifies calcium signaling beyond that observed on flat-ZrOx surfaces.

Together, these data suggest that ns-ZrOx not only supports astrocyte survival and differentiation but also reshapes the

https://doi.org/10.1021/acsabm.6c01280
ACS Appl. Bio Mater. 2026, 9, 8345−8358

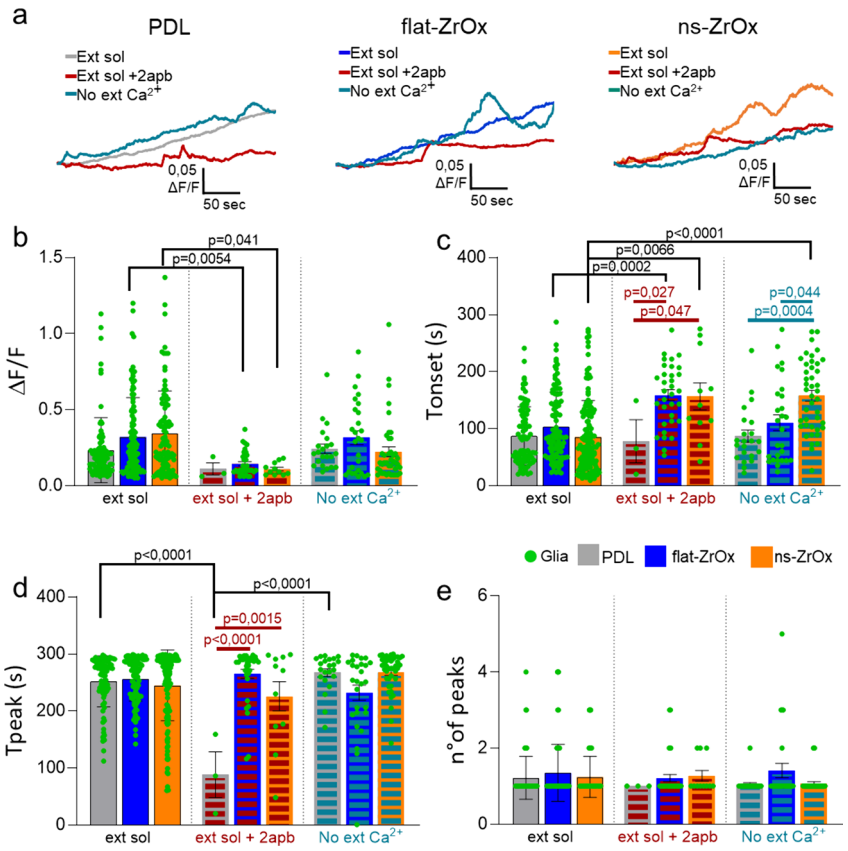

Figure 7. Internal and external calcium contributions to calcium dynamics in DRG glial cells on ZrOx. (a) Representative traces of fluorescence intensity variation (ΔF/F) over time of DRG glia plated on all the substrates in control conditions and following the treatment with 2APB and the removal of external Ca^{2+}. (b) Histogram showing maximum fluorescence intensity values in responding DRG glial cells cultured on PDL, flat-ZrOx, and ns-ZrOx in control conditions, following IP_3 pathway inhibition [ext sol + 2apb: PDL (0.11 ± 0.04, $n = 3$, $N = 3$), flat-ZrOx (0.14 ± 0.014, $n = 33$, $N = 3$), and ns-ZrOx (0.10 ± 0.012, $n = 11$, $N = 3$)], and removal of external Ca^{2+} [No ext Ca^{2+}: PDL (0.24 ± 0.03, $n = 22$, $N = 3$), flat-ZrOx (0.24 ± 0.045, $n = 27$, $N = 3$), and ns-ZrOx (0.22 ± 0.03, $n = 41$, $N = 3$)]. (c) Histogram showing the time onset in responding DRG glial cells cultured on PDL, flat-ZrOx, and ns-ZrOx in control conditions, following IP_3 pathway inhibition [ext sol + 2apb: PDL (78 ± 37.80, $n = 3$, $N = 3$), flat-ZrOx (158.9 ± 9.53, $n = 33$, N = 3), and ns-ZrOx (156.4 ± 23.49, $n = 11$, $N = 3$)], and removal of external Ca^{2+} [No ext Ca^{2+}: PDL (86.68 ± 10.7, $n = 22$, $N = 3$), flat-ZrOx (110.4 ± 13.91, $n = 27$, $N = 3$), and ns-ZrOx (157.5 ± 9.58, $n = 42$, $N = 3$)]. (d) Histogram showing the time to peak in responding DRG glial cells cultured on PDL, flat-ZrOx, and ns-ZrOx in control conditions, following IP_3 pathway inhibition [ext sol + 2apb: PDL (88.33 ± 40.14, $n = 3$, $N = 3$), flat-ZrOx (265.2 ± 8.19, $n = 33$, $N = 3$), and ns-ZrOx (225.7 ± 25.54, $n = 11$, $N = 3$)], and removal of external Ca^{2+} [No ext Ca^{2+}: PDL (267.2 ± 6.88, $n = 22$, $N = 3$), flat-ZrOx (232.1 ± 13.34, $n = 27$, $N = 3$), and ns-ZrOx (267.7 ± 5.31, $n = 41$, $N = 3$)]. (e) Histogram showing the number of peaks in responding DRG glial cells cultured on PDL, flat-ZrOx, and ns-ZrOx in control conditions, following IP_3 pathway inhibition [ext sol + 2apb: PDL (1 ± 0, $n = 3$, $N = 3$), flat-ZrOx (1.21 ± 0.09, $n = 33$, $N = 3$), and ns-ZrOx (1.27 ± 0.14, $n = 11$, $N = 3$)], and removal of external Ca^{2+} [No ext Ca^{2+}: PDL (1.04 ± 0.04, $n = 22$, $N = 3$), flat-ZrOx (1.40 ± 0.18, $n = 27$, $N = 3$), and ns-ZrOx (1.07 ± 0.04, $n = 41$, $N = 3$)]. p values are displayed on the figure.

machinery beyond their signaling toward a more excitable and responsive state. Such modulation may be advantageous for the design of biomaterials intended to recapitulate the dynamic, bidirectional signaling that characterizes tripartite synapses *in vivo*.[2]

To extend our study, we performed biocompatibility and functional experiments using glial and neuronal cells from the PNS, using a co-culture of DRG neuron and glia. The latter represents a model to study neural interfaces with cells of the sensory system.[44] In DRG co-cultures, both neurons and glial cells adhered and survived equally well on all zirconia substrates, confirming the biocompatibility of ZrOx substrates. However, functional imaging revealed that the nanostructured surface selectively enhanced calcium signaling in glial cells, while neuronal activity remained relatively stable across substrates. This selective sensitivity may reflect intrinsic differences in how glia and neurons interact with their microenvironment. Glial cells, being more mechanosensitive and reliant on extracellular cues for calcium wave propagation, likely respond more strongly to the altered topography and surface energy of ns-ZrOx.[45,46] However, previous studies showed that when primary hippocampal neurons are cultured on such cluster-assembled nanostructured zirconia surfaces, they display accelerated maturation, earlier action potential generation, and enhanced spontaneous synaptic activity, meaning that ZrOx modulate the functional network formation.[47] Moreover, DRG neurons cultured on nanostructured silicon nanowire mats demonstrated enhanced preservation of functional and electrophysiological activity compared to conventional substrates.[44]

The persistence of partial calcium signaling on ns-ZrOx after IP_3R blockade, in contrast to its complete suppression on flat-ZrOx and PDL, further highlights the substrate's influence on intracellular signaling routes. This residual activity may involve alternative calcium sources, such as mechanosensitive channels

https://doi.org/10.1021/acsabm.6c01280
ACS Appl. Bio Mater. 2026, 9, 8345−8358

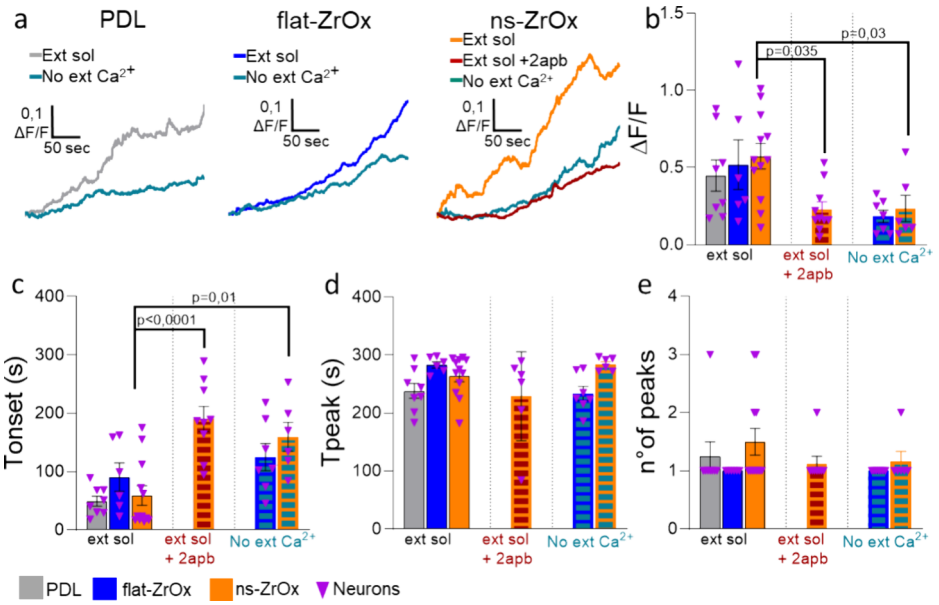

Figure 8. Extracellular calcium contribution on DRG neuronal calcium responses on ZrOx Substrates. (a) Representative traces of fluorescence intensity variation ($\Delta F/F$) over time of DRG neurons plated on all the substrates in control conditions and following 2APB treatment and removal of external Ca^{2+}. Quantitative analyses for PDL and flat-ZrOx groups following IP_3 pathway inhibition and for PDL following extracellular calcium removal were not performed because an insufficient number of cells remained responsive after treatment. (b) Histogram showing maximum fluorescence intensity values in responding DRG neurons cultured on PDL, flat-ZrOx, and ns-ZrOx in control conditions, following 2APB treatment (ns-ZrOx: 0.23 ± 0.04, $n = 9$, $N = 3$), and removal of external Ca^{2+} [flat-ZrOx (0.18 ± 0.040, $n = 7$, $N = 3$) and ns-ZrOx (0.23 ± 0.08, $n = 6$, $N = 3$)]. (c) Histogram showing the time onset in responding DRG neurons cultured on PDL, flat-ZrOx, and ns-ZrOx in control conditions, following 2APB treatment (ns-ZrOx: 190.5 ± 21.43, $n = 9$, $N = 3$), and removal of external Ca^{2+} [flat-ZrOx (124.8 ± 23.34, $n = 7$, $N = 3$) and ns-ZrOx (159.8 ± 24.8, $n = 6$, $N = 3$)]. (d) Histogram showing the time to peak in responding DRG neurons cultured on PDL, flat-ZrOx, and ns-ZrOx in control conditions, following 2APB treatment (ns-ZrOx: 229.2 ± 31.29, $n = 9$, $N = 3$), and removal of external Ca^{2+} [flat-ZrOx (233.9 ± 12.31, $n = 7$, $N = 3$) and ns-ZrOx (284.3 ± 4.63, $n = 6$, $N = 3$)]. (e) Histogram showing the number of peaks in responding DRG neurons cultured on PDL, flatZrOx, and ns-ZrOx in control conditions, following 2APB treatment (ns-ZrOx: 1.125 ± 0.12, $n = 9$, $N = 3$), and removal of external Ca^{2+} [flat-ZrOx (1 ± 0, $n = 7$, $N = 3$) and ns-ZrOx (1.16 ±0.16, $n = 6$, $N = 3$)]. p values are displayed on the figure.

or store-operated calcium entry (SOCE), whose function could be enhanced by nanoscale features.[48] Similarly, in calcium-free conditions, ns-ZrOx induced distinct temporal changes in both neuronal and glial populations, suggesting that the surface can tune the balance between extracellular influx and intracellular release mechanisms.

These results collectively indicate that ns-ZrOx acts as an active neuromorphic interface, capable of modulating not only neuronal but also glial excitability. The fact that such modulation is consistent across both CNS and PNS cell types underscores the robustness and versatility of zirconia as a glio-compatible material.

Traditionally, materials and systems for neuromorphic computing have focused primarily on mimicking neuronal behavior, replicating spiking, synaptic plasticity. Emerging evidence shows that glial cells play equally critical roles in regulating network excitability and information processing.[49−51] By demonstrating that ns-ZrOx can differentially affect neuron–glia communication, this study supports the development of glio-neuromorphic interfaces, which integrate both neuronal and glial components to better emulate the complexity of biological information processing.

Moreover, astrocyte-inspired zirconia-based memristive devices have recently been shown to exhibit recoverable conductance linearity and enhanced learning performance, demonstrating how astrocytic principles can be directly translated into hardware implementations to stabilize and improve neuromorphic computation.[52]

The enhanced calcium signaling observed on ns-ZrOx suggests that such substrates can be implemented in hybrid systems that couple living glial–neuronal networks with artificial neuromorphic devices. In particular, the application of modulated electrical stimuli by the substrates and the recording and processing of cell responses by means of the resistive switching activity of the nanostructured material itself can foster neurogliomorphic bidirectional communication between the artificial and living neural networks in real-time and integrated directly into the culture Petri dish. The previously described complex electrical behavior of ns-ZrOx further reinforces this possibility, indicating that these materials could serve not only as biocompatible scaffolds but also as functional components to actively induce signal processing in both neurons and astrocytes.

More broadly, these findings support an interdisciplinary view of neuromorphic systems in which biological function and device physics must be jointly considered.[53] In this framework, our study provides a direct experimental bridge between glial physiology and nanoscale material properties, positioning nanostructured cluster-assembled thin films as a key enabling platform for next-generation glio-neuromorphic systems.

■ CONCLUSIONS

In this work, we propose and identify ns-ZrOx as a neurogliomorphic interface capable of actively shaping neuroglial function. Beyond its high biocompatibility, ns-ZrOx selectively enhances glial calcium dynamics while eliciting distinct responses in neuronal populations. Importantly, our findings show that the effects induced by ns-ZrOx substrates are conserved across both central

https://doi.org/10.1021/acsabm.6c01280
ACS Appl. Bio Mater. 2026, 9, 8345−8358

and peripheral neuroglial systems, indicating that the influence of nanoscale topography on calcium-dependent signaling represents a robust and generalizable phenomenon rather than a specific response. The observation that ns-ZrOx selectively potentiates glial excitability, while preserving neuronal viability and activity, further supports the concept that glial cells constitute highly responsive targets for neuromorphic material engineering. In this context, ns-ZrOx does not merely function as a passive scaffold, but rather as an active neuroglial interface capable of modulating intracellular signaling pathways and neuroglial communication. These features are particularly relevant for the development of hybrid bioelectronic systems, where the bidirectional interaction between living neural networks and advanced materials requires dynamic and adaptive functional capabilities.

Overall, this work contributes to a broader shift from neuron-centered approaches toward integrated neuron–glia paradigms that more faithfully reproduce the emergent properties of biological neural networks.[54,55] By bridging glial physiology and neuromorphic nanostructured materials, our study establishes cluster-assembled zirconia thin films as a promising platform for next-generation biohybrid technologies, including adaptive neural interfaces, brain-inspired computing architectures, and real-time neuroelectronic communication systems.

AUTHOR INFORMATION

Corresponding Authors

Giorgia Conte – *Consiglio Nazionale delle Ricerche, Istituto per la Sintesi Organica e la Fotoreattività, Bologna 40129, Italy;* orcid.org/0000-0003-0566-9339; Email: giorgia.conte@cnr.it

Paolo Milani – *CIMAINA and Dipartimento di Fisica "A. Pontremoli", Università degli Studi di Milano, Milan 20133, Italy;* Email: pmilani@mi.infn.it

Valentina Benfenati – *Consiglio Nazionale delle Ricerche, Istituto per la Sintesi Organica e la Fotoreattività, Bologna 40129, Italy;* Email: valentina.benfenati@cnr.it

Authors

Francesca Borghi – *CIMAINA and Dipartimento di Fisica "A. Pontremoli", Università degli Studi di Milano, Milan 20133, Italy;* orcid.org/0000-0001-6980-4910

Chiara Lazzarini – *Consiglio Nazionale delle Ricerche, Istituto per la Sintesi Organica e la Fotoreattività, Bologna 40129, Italy; Department of Biosciences, Biotechnology and Environment, University of Bari Aldo Moro, Bari 70121, Italy*

Claudio Piazzoni – *CIMAINA and Dipartimento di Fisica "A. Pontremoli", Università degli Studi di Milano, Milan 20133, Italy*

Aikaterini Konstantoulaki – *Consiglio Nazionale delle Ricerche, Istituto per la Sintesi Organica e la Fotoreattività, Bologna 40129, Italy*

Roberta Fabbri – *Consiglio Nazionale delle Ricerche, Istituto per la Sintesi Organica e la Fotoreattività, Bologna 40129, Italy*

Marco Caprini – *Department of Pharmacy and Biotechnology (FaBit), University of Bologna, Bologna 40126, Italy; Istituto delle Scienze Neurologiche di Bologna, Bologna 40124, Italy*

Complete contact information is available at: https://pubs.acs.org/doi/10.1021/acsabm.6c01280

Author Contributions

[†]G.C., F.B., P.M., and V.B. contributed equally to this work. The manuscript was written through contributions of all authors. All authors have given approval to the final version of the manuscript. V.B., P.M., G.C., and F.B. conceived and designed the experiments. C.P. fabricated flat- and ns-ZrOx substrates. F.B. characterized the substrates. G.C. and C.L. performed immunofluorescence characterization, viability test, and calcium imaging and analyzed the related data. G.C., C.L., A.K. and R.F. prepared and maintained the astrocytes and DRG cell culture. M.C. supported the preparation of the cell cultures. G.C. wrote the manuscript. All authors discussed the results and contributed to the manuscript writing and reviewing.

Funding

This work was financially supported by US ARO ASTRO-CLUSTER, W911NF2520009, and by US Air Force of Scientific Research-AFOSR projects and ASTROTALK-FA9550-23-1-0736 and ASTROSENSE FA9550-25-1-0001. G.C. acknowledged the financial support from PNRR MUR project ECS_00000033_ECOSISTER. P.M. and F.B. acknowledged the financial support by Regione Lombardia under the PR FESR 2021-2027 programme, 'Collabora & Innova' initiative, Project (SMARTSPINE/CUP: E29I25000730007).

Notes

The authors declare no competing financial interest.

ABBREVIATIONS

ZrOx	zirconium oxide
ns	nanostructured
DRG	dorsal root ganglion
($[Ca^{2+}]_i$)	intracellular calcium signaling
ECM	extracellular matrix
ns-ZrOx/Au	nanostructured zirconia and gold
SCBD	supersonic cluster beam deposition
PMCS	pulsed microplasma cluster source
Rq	roughness
AFM	atomic force microscopy
DMEM	Dulbecco's modified Eagle medium
FBS	fetal bovine serum
FDA	fluorescent diacetate assay
PDL	poly-D-lysine
DIV	days in vitro
2APB	2-aminoethyl diphenylborinate
IP3	inositol 1,4,5-trisphosphate
($0Ca^{2+}$)	calcium-free extracellular saline
CNS	central nervous system
PNS	peripheral nervous system
GAP-43	growth-associated protein-43
SOCE	store-operated calcium entry

REFERENCES

(1) Verkhratsky, A.; Parpura, V.; Vardjan, N.; Zorec, R. Physiology of Astroglia. *Adv. Exp. Med. Biol.* **2019**, *1175*, 45–91.

(2) Volterra, A.; Meldolesi, J. Astrocytes, from Brain Glue to Communication Elements: The Revolution Continues. *Nat. Rev. Neurosci.* **2005**, *6* (8), 626–640.

(3) Perea, G.; Araque, A. Astrocytes Potentiate Transmitter Release at Single Hippocampal Synapses. *Science* **2007**, *317* (5841), 1083–1086.

(4) Araque, A.; Parpura, V.; Sanzgiri, R. P.; Haydon, P. G. Tripartite Synapses: Glia, the Unacknowledged Partner. *Trends Neurosci.* **1999**, *22* (5), 208–215.
(5) Khakh, B. S.; Sofroniew, M. V. Diversity of Astrocyte Functions and Phenotypes in Neural Circuits. *Nat. Neurosci.* **2015**, *18* (7), 942–952.
(6) Berridge, M. J. Neuronal Calcium Signaling. *Neuron* **1998**, *21* (1), 13–26.
(7) Previdi, A.; Borghi, F.; Profumo, F.; Schulte, C.; Piazzoni, C.; Lamanna, J.; Racchetti, G.; Malgaroli, A.; Milani, P. Nanotopography and Microconfinement Impact on Primary Hippocampal Astrocyte Morphology, Cytoskeleton and Spontaneous Calcium Wave Signalling. *Cells* **2023**, *12* (2), No. 293.
(8) Huo, Z.; Yang, W.; Harati, J.; Nene, A.; Borghi, F.; Piazzoni, C.; Milani, P.; Guo, S.; Galluzzi, M.; Boraschi, D. Biomechanics of Macrophages on Disordered Surface Nanotopography. *ACS Appl. Mater. Interfaces* **2024**, *16* (21), 27164–27176.
(9) Schulte, C.; Rodighiero, S.; Cappelluti, M. A.; Puricelli, L.; Maffioli, E.; Borghi, F.; Negri, A.; Sogne, E.; Galluzzi, M.; Piazzoni, C.; Tamplenizza, M.; Podestà, A.; Tedeschi, G.; Lenardi, C.; Milani, P. Conversion of Nanoscale Topographical Information of Cluster-Assembled Zirconia Surfaces into Mechanotransductive Events Promotes Neuronal Differentiation. *J. Nanobiotechnol.* **2016**, *14* (1), No. 18.
(10) Profumo, F.; Borghi, F.; Falqui, A.; Milani, P. Potentiation and Depression Behaviour in a Two-Terminal Memristor Based on Nanostructured Bilayer ZrOx/Au Films. *J. Phys. D: Appl. Phys.* **2023**, *56* (35), No. 355301.
(11) Profumo, F.; Borghi, F.; Angì, T.; Maschietto, M.; Vassanelli, S.; Milani, P. Highly Efficient Classification of Time-Series Based on Resistive Switching Cluster-Assembled Materials. *Advanced Intelligent Systems* **2025**, *7*, No. e202401150.
(12) Borghi, F.; Nieus, T. R.; Galli, D. E.; Milani, P. Brain-like Hardware, Do We Need It?. *Front. Neurosci.* **2024**, *18*, No. 1465789.
(13) Nadalini, G.; Borghi, F.; Košutová, T.; Falqui, A.; Ludwig, N.; Milani, P. Engineering the Structural and Electrical Interplay of Nanostructured Au Resistive Switching Networks by Controlling the Forming Process. *Sci. Rep.* **2023**, *13* (1), No. 19713.
(14) Podestà, A.; Borghi, F.; Indrieri, M.; Bovio, S.; Piazzoni, C.; Milani, P. Nanomanufacturing of Titania Interfaces with Controlled Structural and Functional Properties by Supersonic Cluster Beam Deposition. *J. Appl. Phys.* **2015**, *118* (23), No. 234309.
(15) Carbone, R.; Marangi, I.; Zanardi, A.; Giorgetti, L.; Chierici, E.; Berlanda, G.; Podestà, A.; Fiorentini, F.; Bongiorno, G.; Piseri, P.; Pelicci, P. G.; Milani, P. Biocompatibility of Cluster-Assembled Nanostructured TiO2 with Primary and Cancer Cells. *Biomaterials* **2006**, *27* (17), 3221–3229.
(16) Mirigliano, M.; Borghi, F.; Podestà, A.; Antidormi, A.; Colombo, L.; Milani, P. Non-Ohmic Behavior and Resistive Switching of Au Cluster-Assembled Films beyond the Percolation Threshold. *Nanoscale Adv.* **2019**, *1* (8), 3119–3130.
(17) Cipollini, D.; Profumo, F.; Schomaker, L.; Milani, P.; Borghi, F. Conduction Mechanisms in a Planar Nanocomposite Resistive Switching Device Based on Cluster-Assembled Au/ZrOx Films. *Front. Mater.* **2024**, *11*, No. 1385792.
(18) Decastri, D.; Nieus, T.; Zuccali, C.; Giacomozzi, F.; Lorenzelli, L.; Borghi, F.; Milani, P. Programmable Functional Connectivity and Synchronous Activity in Resistive Switching Self-Assembled Nanostructured Networks. *Small Struct.* **2025**, *6* (11), No. 2500330.
(19) Nadalini, G.; Dallinger, A.; Sottocorno, D.; Greco, F.; Borghi, F.; Milani, P. Soft Electronic Switches and Adaptive Logic Gates Based on Nanostructured Gold Networks. *Adv. Electron. Mater.* **2025**, *11* (7), No. 2400717.
(20) Nadalini, G.; Milani, P.; Borghi, F. In-Sensor Computing by Soft Threshold Logic Gates Under Different Humidity Conditions *Adv. Electron. Mater.* **2026**, e00863.
(21) Sarnthein, J.; Neidert, M. C. A Profile on the WISE Cortical Strip for Intraoperative Neurophysiological Monitoring. *Expert Rev. Med. Devices* **2024**, *21* (5), 373–379.
(22) Biagioli, N.; Morandi, S.; Vaudano, A. E.; Pugnaghi, M.; Moriconi, E.; Pavesi, G.; Tramontano, V.; Meletti, S. Intraoperative ECoG in Bottom-of-the-Sulcus Syndrome Using a Novel Flexible Strip Electrode. *Epileptic Disord.* **2024**, *26* (3), 357–364.
(23) Barborini, E.; Kholmanov, I. N.; Conti, A. M.; Piseri, P.; Vinati, S.; Milani, P.; Ducati, C. Supersonic Cluster Beam Depositionof Nanostructured Titania. *Eur. Phys. J. D* **2003**, *24* (1), 277–282.
(24) Wegner, K.; Piseri, P.; Tafreshi, H. V.; Milani, P. Cluster Beam Deposition: A Tool for Nanoscale Science and Technology. *J. Phys. D: Appl. Phys.* **2006**, *39* (22), R439–R459.
(25) Borghi, F.; Sogne, E.; Lenardi, C.; Podestà, A.; Merlini, M.; Ducati, C.; Milani, P. Cluster-Assembled Cubic Zirconia Films with Tunable and Stable Nanoscale Morphology against Thermal Annealing. *J. Appl. Phys.* **2016**, *120* (5), No. 055302.
(26) Borghi, F.; Podestà, A.; Piazzoni, C.; Milani, P. Growth Mechanism of Cluster-Assembled Surfaces: From Submonolayer to Thin-Film Regime. *Phys. Rev. Appl.* **2018**, *9* (4), No. 044016.
(27) Pazyra-Murphy, M. F.; Segal, R. A. Preparation and Maintenance of Dorsal Root Ganglia Neurons in Compartmented Cultures *J. Visualized Exp.* **2008**, No. *20*, e951.
(28) Galland, F.; Seady, M.; Taday, J.; Smaili, S. S.; Gonçalves, C. A.; Leite, M. C. Astrocyte Culture Models: Molecular and Function Characterization of Primary Culture, Immortalized Astrocytes and C6 Glioma Cells. *Neurochem. Int.* **2019**, *131*, No. 104538.
(29) Collon, K.; Bell, J. A.; Chang, S. W.; Gallo, M. C.; Sugiyama, O.; Marks, C.; Lieberman, J. R. Effects of Cell Seeding Technique and Cell Density on BMP-2 Production in Transduced Human Mesenchymal Stem Cells. *J. Biomed. Mater. Res., Part A* **2022**, *110* (12), 1944–1952.
(30) Issa, R. I.; Engebretson, B.; Rustom, L.; McFetridge, P. S.; Sikavitsas, V. I. The Effect of Cell Seeding Density on the Cellular and Mechanical Properties of a Mechanostimulated Tissue-Engineered Tendon. *Tissue Eng., Part A* **2011**, *17* (11–12), 1479–1487.
(31) Huang, J.; Chen, Y.; Tang, C.; Fei, Y.; Wu, H.; Ruan, D.; Paul, M. E.; Chen, X.; Yin, Z.; Heng, B. C.; Chen, W.; Shen, W. The Relationship between Substrate Topography and Stem Cell Differentiation in the Musculoskeletal System. *Cell. Mol. Life Sci.* **2018**, *76* (3), 505–521.
(32) Blumenthal, N. R.; Hermanson, O.; Heimrich, B.; Shastri, V. P. Stochastic Nanoroughness Modulates Neuron–Astrocyte Interactions and Function via Mechanosensing Cation Channels. *Proc. Natl. Acad. Sci.* **2014**, *111* (45), 16124–16129.
(33) Saracino, E.; Maiolo, L.; Polese, D.; Semprini, M.; Borrachero-Conejo, A. I.; Gasparetto, J.; Murtagh, S.; Sola, M.; Tomasi, L.; Valle, F.; Pazzini, L.; Formaggio, F.; Chiappalone, M.; Hussain, S.; Caprini, M.; Muccini, M.; Ambrosio, L.; Fortunato, G.; Zamboni, R.; Convertino, A.; Benfenati, V. A Glial-Silicon Nanowire Electrode Junction Enabling Differentiation and Noninvasive Recording of Slow Oscillations from Primary Astrocytes. *Adv. Biosyst.* **2020**, *4* (4), No. 1900264.
(34) Posati, T.; Pistone, A.; Saracino, E.; Formaggio, F.; Mola, M. G.; Troni, E.; Sagnella, A.; Nocchetti, M.; Barbalinardo, M.; Valle, F.; Bonetti, S.; Caprini, M.; Nicchia, G. P.; Zamboni, R.; Muccini, M.; Benfenati, V. A Nanoscale Interface Promoting Molecular and Functional Differentiation of Neural Cells. *Sci. Rep.* **2016**, *6* (1), No. 31226.
(35) Takata, N.; Mishima, T.; Hisatsune, C.; Nagai, T.; Ebisui, E.; Mikoshiba, K.; Hirase, H. Astrocyte Calcium Signaling Transforms Cholinergic Modulation to Cortical Plasticity in Vivo. *J. Neurosci.* **2011**, *31* (49), 18155–18165.
(36) Grafe, I.; Alexander, S.; Peterson, J. R.; Snider, T. N.; Levi, B.; Lee, B.; Mishina, Y. TGF-β Family Signaling in Mesenchymal Differentiation. *Cold Spring Harbor Perspect. Biol.* **2018**, *10* (5), No. a022202.
(37) Salasznyk, R. M.; Klees, R. F.; Williams, W. A.; Boskey, A.; Plopper, G. E. Focal Adhesion Kinase Signaling Pathways Regulate the Osteogenic Differentiation of Human Mesenchymal Stem Cells. *Exp. Cell Res.* **2007**, *313* (1), 22–37.

https://doi.org/10.1021/acsabm.6c01280
ACS Appl. Bio Mater. 2026, 9, 8345–8358

(38) Sachdev, P.; Zeng, L.; Wang, L. H. Distinct Role of Phosphatidylinositol 3-Kinase and Rho Family GTPases in Vav3-Induced Cell Transformation, Cell Motility, and Morphological Changes*. *J. Biol. Chem.* **2002**, *277* (20), 17638–17648.
(39) Pirri, C. PIEZO Channels in Mechano-Inflammation: Gatekeepers of Neuroimmune Crosstalk. *Diseases* **2025**, *13* (8), No. 263.
(40) Uray, I. P.; Uray, K. Mechanotransduction at the Plasma Membrane-Cytoskeleton Interface. *Int. J. Mol. Sci.* **2021**, *22* (21), No. 11566.
(41) Perea, G.; Araque, A. GLIA Modulates Synaptic Transmission. *Brain Res. Rev.* **2010**, *63* (1), 93–102.
(42) Fabbri, R.; Spennato, D.; Conte, G.; Konstantoulaki, A.; Lazzarini, C.; Saracino, E.; Nicchia, G. P.; Frigeri, A.; Zamboni, R.; Spray, D. C.; Benfenati, V. The Emerging Science of Glioception: Contribution of Glia in Sensing, Transduction, Circuit Integration of Interoception. *Pharmacol. Ther.* **2023**, *245*, No. 108403.
(43) Benowitz, L. I.; Routtenberg, A. GAP-43: An Intrinsic Determinant of Neuronal Development and Plasticity. *Trends Neurosci.* **1997**, *20* (2), 84–91.
(44) Lucarini, I.; Maita, F.; Conte, G.; Saracino, E.; Formaggio, F.; Palmieri, E.; Fabbri, R.; Konstantoulaki, A.; Lazzarini, C.; Caprini, M.; Benfenati, V.; Maiolo, L.; Convertino, A. Silicon Nanowire Mats Enable Advanced Bioelectrical Recordings in Primary DRG Cell Cultures. *Adv. Healthcare Mater.* **2025**, *14* (17), No. 2500379.
(45) Marinval, N.; Chew, S. Y. Mechanotransduction Assays for Neural Regeneration Strategies: A Focus on Glial Cells. *APL Bioeng* **2021**, *5* (2), No. 021505.
(46) Barnes, J. M.; Przybyla, L.; Weaver, V. M. Tissue Mechanics Regulate Brain Development, Homeostasis and Disease. *J. Cell Sci.* **2017**, *130* (1), 71–82.
(47) Schulte, C.; Ripamonti, M.; Maffioli, E.; Cappelluti, M. A.; Nonnis, S.; Puricelli, L.; Lamanna, J.; Piazzoni, C.; Podestà, A.; Lenardi, C.; Tedeschi, G.; Malgaroli, A.; Milani, P. Scale Invariant Disordered Nanotopography Promotes Hippocampal Neuron Development and Maturation with Involvement of Mechanotransductive Pathways. *Front. Cell. Neurosci.* **2016**, *10*, No. 267.
(48) Zhang, Y.; Li, K.; Li, G. Investigation of Nanotopography on SOCE Mediated Cell Migration via Live-Cell Imaging on Opaque Implant Surface. *J. Nanobiotechnol.* **2023**, *21*, 471.
(49) Peng, H.-R.; Zhang, Y.-K.; Zhou, J.-W. The Structure and Function of Glial Networks: Beyond the Neuronal Connections. *Neurosci. Bull.* **2022**, *39* (3), 531–540.
(50) Kettenmann, H.; Verkhratsky, A. Neuroglia, der lebende Nervenkitt. *Fortschr. Neurol. Psychiatr.* **2011**, *79* (10), 588–597.
(51) Jäkel, S.; Dimou, L. Glial Cells and Their Function in the Adult Brain: A Journey through the History of Their Ablation. *Front. Cell. Neurosci.* **2017**, *11*, No. 24.
(52) Cheng, C.; Wang, Y.; Xu, L.; Liu, K.; Dang, B.; Lu, Y.; Yan, X.; Huang, R.; Yang, Y. Artificial Astrocyte Memristor with Recoverable Linearity for Neuromorphic Computing. *Adv. Electron. Mater.* **2022**, *8* (8), No. 2100669.
(53) Giugliano, M.; Bisquert, J.; Milić, J. V. Across Disciplines of Emerging Neuromorphic Systems: From Neuroscience to Physical Chemistry of Materials and Devices*. *J. Phys. Mater.* **2025**, *9* (1), No. 011002.
(54) Maiolo, L.; Guarino, V.; Saracino, E.; Convertino, A.; Melucci, M.; Muccini, M.; Ambrosio, L.; Zamboni, R.; Benfenati, V. Glial Interfaces: Advanced Materials and Devices to Uncover the Role of Astroglial Cells in Brain Function and Dysfunction. *Adv. Healthcare Mater. 2021*, *10* (1), e2001268.
(55) Benfenati, V.; Maiolo, L. Eds. Glial Engineering and Glial Interfaces: Targeting the Role of Astrocytes and Other Glial Cells in Brain Function and Dysfunctions; Springer: Cham, Switzerland, **2025**.

https://doi.org/10.1021/acsabm.6c01280
ACS Appl. Bio Mater. 2026, 9, 8345−8358